Ocean Engineering 207 (2020) 107385

Contents lists available at ScienceDirect

Ocean Engineering

journal homepage: www.elsevier.com/locate/oceaneng

Investigation of harbor oscillations originated from the vessel-induced bores using methods of autoregressive model and Mahalanobis distance

Dong Shao [a], Yun Xing [b,*], Zirui Zheng [c], Gang Jiang [a]

[a] College of Transportation Science and Engineering, Nanjing Tech University, Nanjing, 210009, China
[b] Key Laboratory of Meteorological Disaster, Ministry of Education, Joint International Research Laboratory of Climate and Environment Change, Collaborative Innovation Centre on Forecast and Evaluation of Meteorological Disasters, School of Hydrology and Water Resources, Nanjing University of Information Science and Technology, Nanjing, 210044, China
[c] Heinz College of Information Systems and Public Policy, Carnegie Mellon University, Pittsburgh, PA, 15213-3890, USA

A R T I C L E I N F O

Keywords:
Harbor oscillations
Vector autoregressive model
Statistical pattern recognition
Numerical experiments

A B S T R A C T

This paper presents a study for investigating and identifying features of oscillation patterns induced by vessel motions in the context of statistical pattern recognition on the basis of time-domain oscillation series in addition to traditional frequency-domain analysis. Numerical simulations are carried out for a semi-enclosed harbor of variable depth with different vessel motions as external agitation sources and the oscillation responses are measured at multiple locations along the backwall in the longshore direction and along one sidewall in the offshore direction. Vector autoregressive type models are proposed and applied on the recorded oscillation time series. From clustering of the selected vector autoregressive model coefficients fitted to the oscillation responses, both the influences of a changing bathymetry and those of various vessel motions can be recognized, although some of them are insensitive to frequency-domain analysis and cannot be revealed with the amplitude spectra. With Mahalanobis distances calculated from the spatially distributed measurements at observation points within the harbor, an insight into the internal structure and energy distribution of the vessel-induced oscillations can be achieved by extracting the probability density distributions and the occurrence or absence of certain oscillation components or modes can be analyzed with the proposed pattern recognition approach.

1. Introduction

Oscillations due to the trapping and amplifying effects of a semi-enclosed area with variable water depth such as a bay or a harbor may cause transient destructive effects with their non-trapped modes or long-lasting detrimental effects with their trapped modes. By inducing intolerable vessel motions and inacceptable wave force upon the marine structures within the semi-enclosed area, harbor oscillations may lead to severe problems such as interruption of cargo operations, excessive forces within mooring ropes, overturning of vessels and even damage or failure of marine structures. While the oscillation events as a suffering of many harbors around the world are reported in continuance (Chen et al., 2004; González-Marco et al., 2008; Kofoed-Hansen et al., 2005; Kumar 2017; Kumar et al. 2014, 2016), investigations about their associated hydrodynamic phenomena and wave patterns are worth further concerns in both engineering and scientific aspects.

Research efforts have been made in the first place for harbor oscillations generated by external forcing coming from the open sea outside of the semi-enclosed harbor area and both stationary and transient ones have been studied (Chen et al., 2006; De Girolamo, 1996; Dong et al., 2010a; Gao et al., 2019b; Losada et al., 2008; Mei and Agnon, 1989; Vanoni and Carr, 1950). Investigations have also been carried out for the oscillations induced with the occurrence of inner-harbor agitation forces including submarine landslides, seafloor movements, atmospheric pressures, water surface disturbance etc. (Gao et al., 2018b; Kulikov et al., 1996; Shao et al. 2016, 2017b; Wang et al., 2011; Yalciner and Pelinovsky, 2007). For harbor oscillations induced by various external forces or on different bathymetries, frequency-domain approaches such as spectra analysis are widely employed in the investigations based on the assumption of a quasi-linear expansion of the stochastic moving water surface of the oscillations as a system of independent random variables (Bellotti, 2007; Dong et al., 2010a; Gao et al. 2017, 2018a, 2019a; Kakinuma et al., 2009; Kumar et al., 2016; Rabinovich, 2010; Shao et al., 2017b; Thotagamuwage and

* Corresponding author.
E-mail address: yxing@nuist.edu.cn (Y. Xing).

https://doi.org/10.1016/j.oceaneng.2020.107385
Received 28 October 2019; Received in revised form 20 March 2020; Accepted 12 April 2020
Available online 30 April 2020

Pattiaratchi, 2014a; Wang et al., 2011). With field observations or simulations utilizing well-developed numerical models, water level measurements of harbor oscillations have been extracted at a certain number of observation points as basic data for analysis. In general, the frequency-domain analysis is carried out based on the records of the oscillating water surface when it turns into a quasi-steady state. Together with the frequency-domain analysis, some time-domain attempts have also been made in analyzing harbor oscillation series for their evolution over time by mainly taking advantage of wavelet analysis or even artificial intelligence methods (Dong et al., 2010b; Gao et al., 2016; Kankal and Yüksek, 2012, 2014; Londhe and Deo, 2004; Thotagamuwage and Pattiaratchi, 2014b).

For the time series analysis, autoregressive models have been successfully applied to the structural mechanics in the first place and then to hydrodynamics. With vibration-based structure detections, coefficients of autoregressive models have been used for the extraction of structural features in different conditions including damaged and undamaged ones (Carden and Brownjohn, 2008; Das et al., 2016; Gul and Catbas, 2011; Hoell and Omenzetter, 2016; Sohn et al., 2000; Zhang et al., 2018). Spatial information about the features can also be provided with an analysis of the vibration response of the structure measured at multiple locations and in this regard, vector autoregressive models and moving average ones may have the potential to be used in the spatial identification of the features (Bodeux and Golinval, 2003; Carden and Brownjohn, 2008; Gul and Catbas, 2009; Heyns, 1997; Jayawardhana et al., 2015; Owen et al., 2001; Yao and Pakzad, 2012). In addition to the success of the autoregressive models in structural analysis, the same kinds of time series models have also been applied in hydrodynamic domain and utilized for representing and analyzing metocean variables together with floating body dynamics including the motions of ships and wave energy converters (Degtyarev and Gankevich 2015, 2019; Degtyarev et al., 2019; Fusco and Ringwood, 2010; Gankevich and Degtyarev, 2018; Jäger et al., 2019; Reed et al., 2016; Vanem and Walker, 2013). Hydrodynamic features in both spatial and temporal aspects can be extracted with the application of autoregressive models and on account of that, predictions can be made in a data-driven manner instead of time-consuming numerical simulations. An analysis applied directly on the instantaneously recorded harbor oscillation patterns in time domain may be profitable to investigate the time series mostly with non-stationary nature and extricate us from the limitations of assumed stationarity and small-amplitude wave theory which are generally the basis of frequency domain analysis of wave patterns. As the autoregressive-kind models have been proved to be able to capture the characteristics of propagating wave profiles and their evolutions, they may present an efficient tool for the time series analysis of the harbor oscillation problems with their computational performance.

This paper presents a comprehensive study to investigate the harbor oscillations induced by vessel motions with bathymetry effects taken into account. With conventional analysis in frequency domain for the induced harbor oscillations, an analysis method for the time-domain harbor oscillation behavior is proposed in the context of a pattern recognition problem. An overview of the vector autoregressive model is presented in Section 2 together with the proposed diagnosis scheme. Theoretical formulations of harbor oscillations with variable water depth are briefly reviewed in Section 3 before the numerical model simulating the vessel-induced oscillations. The numerical results are compared with theoretical solutions as a validation. More detailed numerical investigations are presented in the following section with considerations of the effects of variations in both regard to the harbor bathymetry and vessel motions. Multivariate autoregressive models are used to predict the oscillation time series recorded from multiple locations within the harbor. Features for different locations are extracted and analyzed with Mahalanobis distances by measuring the amount of variations in the coefficients of vector autoregressive models. Conclusions are drawn in the last section.

2. Pattern recognition procedure

The vector autoregressive moving average model $VARMA\,(p,q)$ is employed in the analysis procedure of the oscillations induced by vessel motions within the semi-enclosed harbor area described in the following sections. The form of the model can be written as

$$y_t = \sum_{i=1}^{p} \Phi_i y_{t-i} + \sum_{j=1}^{q} \Theta_j \varepsilon_{t-j} + \varepsilon_t \tag{1}$$

where $y_t = (y_{1t}, y_{2t}, \dots, y_{nt})^T$ corresponds to as the vector of dependent response variables, and $\varepsilon_t = (\varepsilon_{1t}, \varepsilon_{2t}, \dots, \varepsilon_{nt})^T$ is referred to the vector white noise process. Here the parameters p and q represent orders of the autoregressive and moving average parts of the VARMA model respectively with n representing the number of dependent response variables used in estimating the VARMA model. In this study, n will be the number of observation points where oscillation time history responses have been measured within the harbor. The interpretation of this model is that the response variables, which are water surface responses at different locations, are not only contemporaneously correlated to each other, but also correlated to each other's past values.

The model coefficients in Eq. (1) Φ_i and Θ_j include implicitly information about physical properties of the harbor and the moving vessel. The Φ_i coefficients define the AR function of order p, and can be used to determine the natural frequencies, mode profiles and damping ratios while Θ_j coefficients define the MA function of order q and include information about power of the response in different modes (Pandit and Wu, 1983). Therefore, if only modal properties of the harbor oscillation patterns are required, the water surface response can be modeled exclusively by the AR part of the model and besides which it is possible to express all VARMA models with AR models of infinite order theoretically. Nevertheless, in a practical account, they may be modeled adequately by a finite order series (Box et al., 1994). There are several different criteria such as the Akaike information criterion (AIC) (Ljung, 1987) and Schwarz's Bayesian criterion (SBC) (Schwarz, 1978) that can be checked to suggest the required order of the AR model. By checking the randomness and Gaussianity of the prediction errors through trial and error, the order of the AR model is determined in this study in parallel with these criteria. The VAR model coefficients are estimated with least squares regression and for each set of the harbor oscillation time histories, p matrices will be obtained as components of $\Phi = (\Phi_1, \Phi_2, \dots, \Phi_i, \dots \Phi_p)$ where Φ_i can be given in matrix form as

$$\Phi_i = \begin{bmatrix} \varphi_{11,i} & \varphi_{12,i} & \cdots & \varphi_{1n,i} \\ \varphi_{21,i} & \varphi_{22,i} & \cdots & \varphi_{2n,i} \\ \vdots & \vdots & \ddots & \vdots \\ \varphi_{n1,i} & \varphi_{n2,i} & \cdots & \varphi_{mn,i} \end{bmatrix} \tag{2}$$

While they are related to the mode profiles and modal frequencies (Andersen, 1997; Andersen and Brincker, 1998), the relation between these coefficients and the modal parameters can be expressed by

$$\begin{bmatrix} 0 & I & 0 & \cdot & 0 \\ 0 & 0 & I & \cdot & 0 \\ \cdot & \cdot & \cdot & \cdot & \cdot \\ 0 & 0 & 0 & \cdot & I \\ \Phi_p & \Phi_{p-1} & \Phi_{p-2} & \cdot & \Phi_1 \end{bmatrix} = \Psi \mu \Psi^{-1} \tag{3}$$

With μ and Ψ indicating respectively the eigenvalues and the mode profiles whereas m equals to np.

$$\mu = \mathrm{diag}\{\mu_i\} \tag{4}$$

$$\Psi = \begin{bmatrix} \psi_1 & \cdot & \cdot & \psi_m \\ \mu_1\psi_1 & \cdot & \cdot & \mu_{np}\psi_m \\ \cdot & \cdot & \cdot & \cdot \\ \mu_1^{p-1}\psi_1 & \cdot & \cdot & \mu_{np}^{p-1}\psi_m \end{bmatrix} \tag{5}$$

For the pattern recognition procedure, the diagnosis approach can be divided into several steps, during which the oscillation responses of the harbor obtained at a variety of conditions are indirectly compared to each other by extracting sensitive features revealed by the application of the chosen VARMA models to the observation data and by statistically measuring the deviations that occur in the estimated coefficients of the models due to the underlying mechanisms. Coefficients of the VARMA model include spatiotemporal information about the vessel-induced oscillations and the amount of deviation observed for different harbor or vessel motion conditions may potentially reveal information about the oscillation characteristics. The details are discussed in the following three steps for the pattern recognition procedure of the harbor oscillations induced by vessel motions:

(1) Formation of the observed oscillation sample: The recorded oscillation data at different conditions are divided into smaller data samples in this diagnosis scheme, which leads to obtaining a number of different VARMA models representing the oscillation response of the harbor in smaller data samples rather than fitting one single model to the entire recorded oscillation time history. With this step, the effect of uncertainty in predicting the parameters of VARMA models can be indirectly included in the diagnosis scheme and the generation of a statistical distribution for the extracted features can be generated.
(2) Oscillation data reduction: In this step of the proposed damage diagnosis scheme, the point of importance consists of estimating the parameters of the VARMA models for each data sample generated from the measured data sets. Within the chosen models, the matrix coefficients, particularly the diagonal terms $\varphi_{jj,1}$ and $\varphi_{jj,2}$ from matrices Φ_1 and Φ_2 in Eq. (2), can be used to extract features at different conditions for the harbor affected by vessel-induced bores, since coefficients for recent time lags like Φ_1 and Φ_2 are the most informative about different modes of the oscillations of the free surface within the harbor whereas other terms in the coefficient matrix may include mixed information (Pandit and Wu, 1983). The $\varphi_{jj,1}$ and $\varphi_{jj,2}$ terms calculated from different data samples can be plotted against each other for comparison. The number of data points is equal to the number of segments in the recorded oscillation data in their corresponding condition.
(3) Oscillation feature extraction and statistical evaluation: A statistical measure called Mahalanobis distance was employed to recognize the variation patterns in the selected terms of the VARMA models by measuring the distance between the selected terms corresponding to a condition of interest and thence used to extract the features of oscillations induced by vessel motions. Generally, the Mahalanobis distance of a multivariate potential outlier vector $x = (x_1, x_2, \dots, x_N)^T$ from a group with mean μ and covariance matrix S is given by

$$D_M(x) = \sqrt{(x-\mu)^T S^{-1}(x-\mu)} \tag{6}$$

Statistical evaluation can be carried out on the calculated features in order to identify patterns of the induced harbor oscillations and the evaluation is performed by comparison between the features calculated for a variety of conditions of interest with both the mean and the variance values of the features taken into account. The selected terms of the fitted VARMA models should experience more or less important deviations within the harbor under different conditions since these coefficients are directly related to the oscillation properties according to Eq. (3) ~ (5). The deviations in the fitted model coefficients are captured by taking advantage of Mahalanobis distances with quantifications of the magnitude of the calculated Mahalanobis distances or the variations in the VARMA coefficients.

For a brief verification of the described analysis method, the VARMA models are in the first place applied onto analytical curves and those with Gaussian white noise signals to test their capability in capturing the characteristics of time series. It can be seen in Fig. 1(a) that a white noise sequence is well generated with the AR function of the first order with $\Phi = 0$ and the autocorrelation of the process in Fig. 1(b) is shown to be validated for the Gaussian white noise with a Kronecker delta at the zero lag and a small tail remaining within the upper and lower confidence bounds (presented with dashed lines). In Fig. 2, a sinusoidal curve and another one with damping are perfectly captured by the VARMA models with orders less than five. When a tiny Gaussian white noise sequence is superposed upon the analytical curves, the characteristics of the artificial curves are also well captured with a fitness over 90% with the model orders within one digit.

3. Numerical study and model validation

The numerical investigations of oscillations induced by vessel motions are conducted within relatively idealized bathymetries with a rectangular semi-enclosed harbor geometry and a piecewise seabed consisted of two slopes to better fitting natural coastal conditions. Simulations are carried out with the well-tested FUNWAVE-TVD package developed at the University of Delaware (Kirby et al., 1998). FUNWAVE-TVD is a fully nonlinear Boussinesq wave model with a Godunov-type Riemann solver (Shi et al., 2012b) and developed based on a complete set of fully nonlinear Boussinesq equations with the vertical vorticity correction derived by Chen, (2006) and a time-varying reference elevation introduced by Kennedy et al., (2001). The governing equations of the numerical model are organized in a conservative form to facilitate a hybrid numerical scheme including third-order Runge--Kutta time-stepping (Gottlieb et al., 2001) and MUSCL-TVD scheme of fourth order accuracy (Erduran et al., 2005) within the Riemann solver. The model has been validated against a suite of benchmark test data in coastal applications (Kirby, 2016; Kirby et al., 2013; Lynett et al., 2017; Shi et al., 2012a; Tehranirad et al., 2011). The mass conservation equations are expressed in the following form

$$\eta_t + \nabla\cdot\mathbf{M} = 0 \tag{8}$$

$$\mathbf{M} = H(\mathbf{u}_a + \bar{\mathbf{u}}_2) \tag{9}$$

With η representing the wave surface elevation and $\mathbf{M}$ the mass flux. $\mathbf{u}_\alpha$ and $\bar{\mathrm{u}}_2$ denote the velocity at a reference elevation and the depth averaged $O(\mu^2)$ respectively where dimensionless parameter characterizing frequency dispersion μ is the ratio of the characteristic water depth to a horizontal length. The total depth $H = h + \eta$ with h the still water depth. The conservative form of the depth-integrated horizontal momentum equations is given as

$$\mathbf{M}_t + \nabla\cdot\left[\frac{\mathbf{MM}}{H}\right] + \nabla\left[\frac{1}{2}g\left(\eta^2 + 2h\eta\right)\right] = \mathbf{V}_{dis} + g\eta\nabla h - gH\nabla p_a - S_{\mathrm{brk}} \tag{10}$$

In which the dispersive terms are contained in $\mathbf{V}_{dis}$ (Shi et al. (2012a)) and the pressure source term generating the ship-wake is presented with the third term on the right-hand side. The last term S_{brk} on RHS is the dissipation term related to the artificial eddy viscosity in the same form of Kennedy et al., (2001) in addition to the shallow water equation-based shock-capturing breaker. The eddy viscosity is described by

$$\nu = B\delta^2(h+\eta)\eta_t \tag{11}$$

With δ the mixing length coefficient equivalent to one in this work. For numerical stability, B may vary smoothly from 0 to 1. However, with the

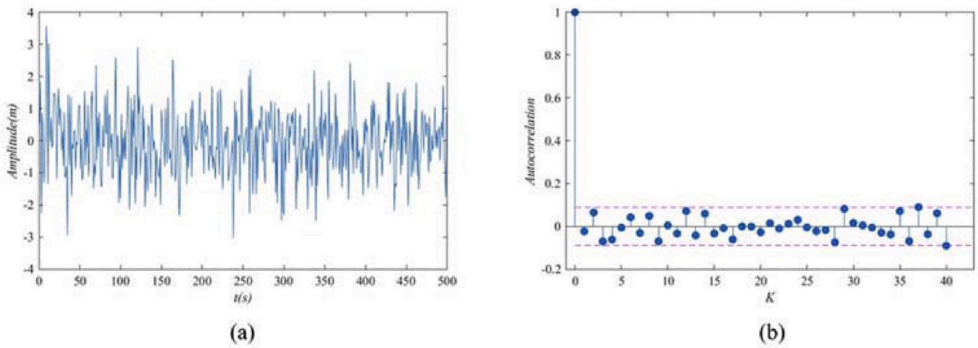

Fig. 1. The Gaussian white noise with the AR function of the first order and its autocorrelation plot with (a) the signal and (b) the stem plot of the autocorrelation with K denoting the lag number.

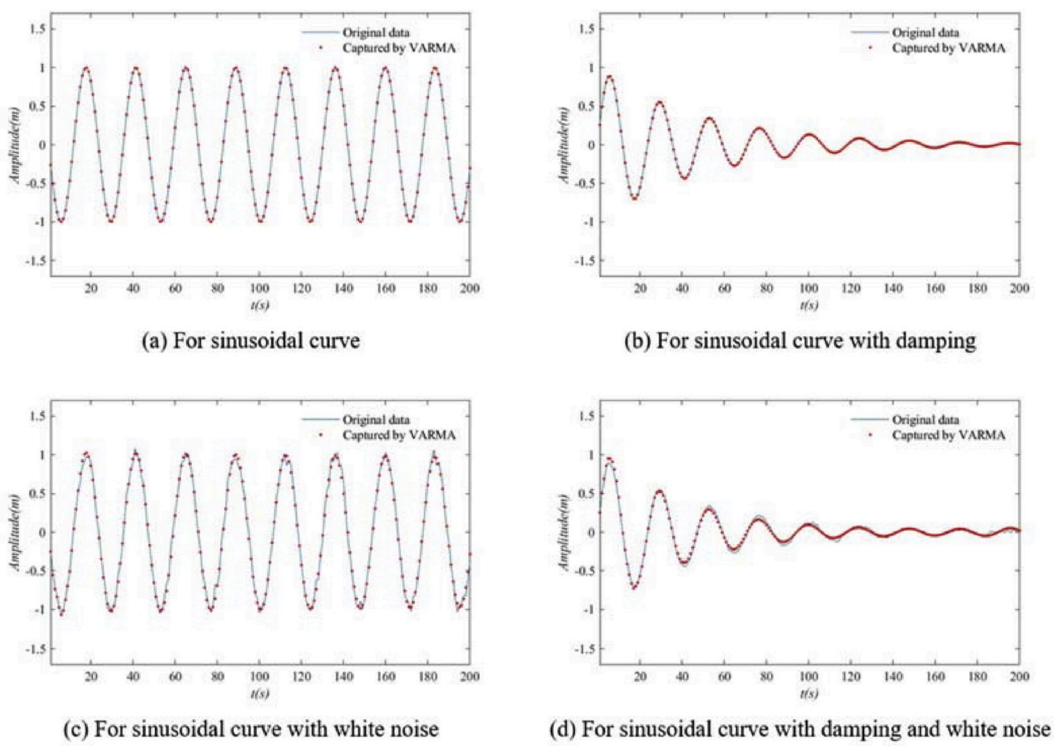

Fig. 2. Comparisons of the artificial curves and the results of the VARMA models.

inherent stability of the TVD numerical scheme, no numerical instability has been found during the simulations in this study without any smooth transition. By adding or flagging out different terms within the source code, FUNWAVE-TVD can be applied as a linear water wave transformation model or to simulate water wave propagations with different levels of Boussinesq approximations with nonlinear terms. The sponge layers of the model package are well validated and can effectively damp the energy of outgoing waves with different frequencies and directions, which is essential for harbor oscillation studies in a numerical manner. In our work, the spongy layers are placed around the boards of the computational domain at a certain distance away from the outlet of the harbor to ensure an open sea condition.

The vessel motions are considered with pressure source for ship-wakes (Ertekin et al., 1986; Torsvik et al., 2008; Wu, 1987) which may be given as

$$p_a(\tilde{x},\tilde{y},t) = Pf(\tilde{x},t)q(\tilde{y},t) \tag{12}$$

Where $p_a(\tilde{x},\tilde{y},t)$ is the static depression around the vessel and P controls the surface displacements which can be interpreted as the inverse barometer effect corresponding to the static surface depression for a stationary vessel. The coordinate system for the pressure source may be rotated by an angle relative to the Boussinesq coordinate system if necessary. With a center point of the pressure located at (x^*,y^*), $f(\tilde{x},t)$ and $q(\tilde{y},t)$ can be expressed respectively as

$$f(\tilde{x},t) = \begin{cases} \cos^2\left[\dfrac{\pi\left(\left|\tilde{x}-x^*(t)\right| - \dfrac{1}{2}\alpha L\right)}{(1-\alpha)L}\right], & \dfrac{1}{2}\alpha L < \left|\tilde{x}-x^*(t)\right| \le \dfrac{1}{2}L \\ 1, & \left|\tilde{x}-x^*(t)\right| \le \dfrac{1}{2}\alpha L \end{cases} \tag{13}$$

$$q(\tilde{y},t)=\begin{cases}\cos^2\left[\dfrac{\pi\left(|\tilde{y}-y^*(t)|-\frac{1}{2}\beta R\right)}{(1-\beta)R}\right], & \frac{1}{2}\beta R<|\tilde{y}-y^*(t)|\le\frac{1}{2}R\\ 1, & |\tilde{y}-y^*(t)|\le\frac{1}{2}\beta R\end{cases}\tag{14}$$

inside the area $-L/2\le\tilde{x}-x^*(t)\le L/2$ and $-R/2\le\tilde{y}-y^*(t)\le R/2$ and their values diminish to zero outside with L and R representing the length and width of the pressure source. The shape of the draft region is determined by the parameters α and β with $0\le(\alpha,\beta)<1$. When the static draft of the vessel is denoted with D, the values of the shape parameters can be evaluated by adjusting them to match the submerged volume of the vessel with a given block coefficient with $C_B = V_{sub}/(L\cdot R\cdot D) = \iint p_a d\tilde{x}d\tilde{y}/(L\cdot R\cdot D)$. The block coefficient can be given as $C_B=0.5$ and the shape parameters are often assumed to be equal with $\alpha=\beta$ in real calculations. In order to carry out investigations of the vessel induced harbor oscillations, the fidelity of the numerical model in simulating the wave patterns generated by moving vessel in depth limited waters is in the first place validated with analytical solution derived by Havelock et al. (Havelock, 1908) as an enhancement of the formulations for Kelvin wake in deep water. Illustrated in Fig. 3(a), the virtual open sea area extends 840 m and 408 m in the longitudinal and the transverse direction respectively with a water depth of 5 m. The vessel moves along the middle axe of the area in the longitudinal direction. The half angles θ_K of the ship wake simulated with Havelock's model setup are compared with the analytical solution with regard to the Froude number (Fr_h) in Fig. 3(b) and the wedges behind the moving vessel are shown to be well captured by the above described numerical model.

For the fidelity of the Boussinesq-type numerical model in the investigation of harbor oscillation problems induced by the vessel-induce bores, the oscillations generated by a moving vessel on two kinds of harbor bathymetries are simulated and compared with the analytical solutions of Shao et al., (2017a) including a constant slope and a two-slope piecewise seabed within the harbor. The computational domain is set up following the usual practice in harbor oscillation researches as shown in Fig. 4 The backwall of the harbor running in the y direction is situated at $x=0$ and x increases offshore. The axis z is positive upward from the still water level. A rectangular harbor of constant slope is located between $x=0$ and $x=L$. The seafloor of the open sea outside the harbor is horizontal. The length of the harbor is relatively long compared with its width $2b$ as evident oscillations frequently occur in long and narrow harbors. In the meantime, as the transverse oscillations may appear in a harbor destabilized by things like small or local disturbances, the harbor width $2b$ may not be too small to restrain their occurrence.

With these considerations, an $L=2.5km$ long and $2b=0.5km$ wide rectangular harbor of conventional dimension is chosen in the numerical simulations for the model validation. Since in a practical account, the speeds of vessels in entering and leaving the harbor are limited according to regulations mainly with security concerns and the vessels may travel at a speed between 5 and $6nmi/h$ (nautical mile per hour) for conventional port waters, a vessel of typical hull form of 20 m long and 10 m wide with $\alpha_v=0.5$ and $\beta_v=0.5$ is set to moving at $5.83nmi/h=10.8km/h$ from the backwall to the mouth of the harbor (namely in the outward direction), which may consequently generate ship-induced bores within the harbor. With results of previous researches of this kind of harbor oscillation problems carried out in recent years, as it is

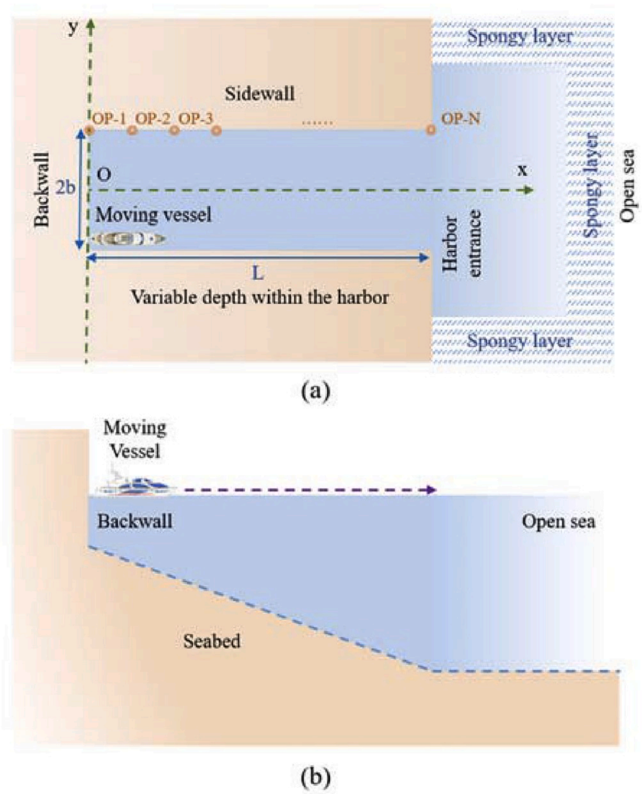

Fig. 4. Definition sketch of the harbor of variable water depth with a vessel traveling along one sidewall of the harbor with (a) the top view and (b) the cross section along the x direction for a constant seabed slope. OP-1 to OP-N indicate the observation points of oscillation measurements along one sidewall.

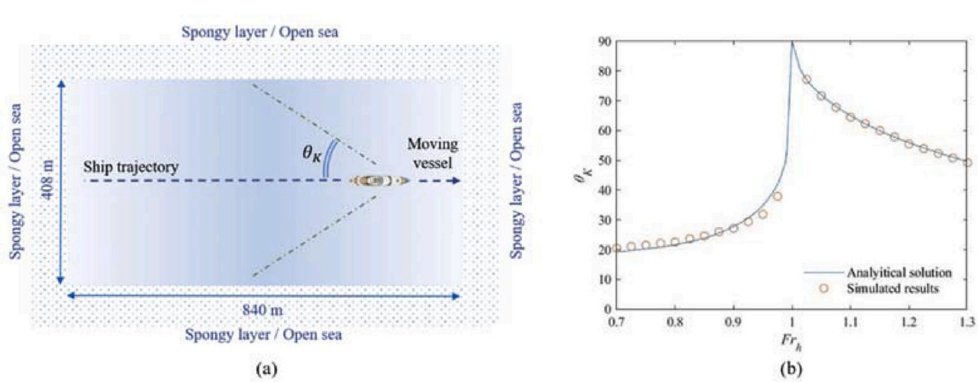

Fig. 3. Comparison of the wedge between the numerical results and the analytical solution of Havelock with regard to different Froude numbers with (a) the model setup and in (b) the blue solid line showing the analytical solution and the numerical results plotted as red circles. (For interpretation of the references to color in this figure legend, the reader is referred to the Web version of this article.)

known that an external disturbance located at or along sidewall of the semi-enclosed harbor area may excite as numerous oscillation modes as possible, the motion path of the vessel is chosen to be along one sidewall of the harbor described above. Oscillations are simulated for the harbor on two kinds of bottom including a constant slope $s = 0.02$ and another one of two-slope-piecewise bottom $s_1 = 0.02,\ \ s_2 = 0.03$ with the same water depth at the back wall $h_1 = 5m$ as validation tests. The piecewise bottom is given by

$$h(x,y) = \begin{cases} s_1 x + h_1 & 0 \le x < x_1 \\ s_2 x + h_2 & x_1 \le x \le L \\ h_p & L < x \end{cases} \tag{15}$$

Where s_1 is the slope of the first part of the bottom and s_2 is that of the second one, with $h_2 = h_1 + (s_1 - s_2)x_1$ the water depth at the point of inflection. The computational domain is $0 \le x \le 3.5$km and -1.25km $\le y \le 1.25$km which dimension the ranges in the longshore and offshore directions in Fig. 4. The grid size is $\Delta x = \Delta y = 5m$ and the time step is $\Delta t = 0.05s$. Three sponge layers of 0.5 km width are placed outside the harbor at a certain distance in the three seaward directions to absorb the energy radiated by the water motion at the entrance. The model is run for sufficiently long time for each simulation as the oscillations within the harbor reach their stable state.

As oscillations of relatively small amplitudes due to the vessel moving with limited speed are focused in this work, the nonlinear interactions between different components can be neglected in the quasi-steady state inside the harbor in assuming the independence of each oscillation component. Following the methods used by Shao et al., (2017b) in analyzing the oscillations induced by submerged sliding masses along the seabed surface, the oscillation components are detected with the amplitude spectra at the corner of the harbor where the amplitude factor of oscillations may attain its maximum. The spatial direction of the oscillations (longitudinal or transverse) is revealed mainly from their profiles in the offshore direction. As indicated in numerous analytical investigations of harbor oscillation, the longitudinal ones have no variation across the harbor but vary along the sidewall whereas the transverse ones have m node lines in parallel with the sidewall and n node lines in parallel with the backwall for the mode (m, n). The spatial structure of each component along the backwall is used to confirm it as longitudinal or transverse. If the motion is transverse, it is further used to identify the value of m corresponding to mode (m,n). The profile of the components along the sidewall is used to identify the mode of the longitudinal oscillation or the offshore node number n of the transverse mode (m,n). Space gauges are installed right at the entrance of the harbor to monitor the energy leaks outside and when it is lower than 0.1% of that contained in the oscillations at the backwall, a quasi-steady state is deemed to be attained. With numerous numerical tests, the oscillations caused by vessel motions are found to be able to reach their quasi-steady state faster for relatively mild seabed than for slightly steeper sloping seabed. The spectra analysis of the simulated free surface elevations is carried out with the time segment after the stabilization of the oscillations with a very large total number of temporal points. The frequency components within the harbor for both the two kinds of bottom are revealed by the amplitude spectrum shown in Fig. 5 and their properties can be further identified from their spatial structure. It can be seen that very weak longitudinal resonances of very low frequency present within the harbor and the wave patterns are controlled by transverse oscillations of different modes. The numerically simulated components frequencies of relatively important intensity and their corresponding theoretical ones calculated from formulations (16) are listed in Table .1 for each case.

$$\begin{aligned}&(U(\alpha_1,1,\tau_{11})U'(\alpha_2,1,\tau_{21}) - U(\alpha_2,1,\tau_{21})U'(\alpha_1,1,\tau_{11}))(2M'(\alpha_1,1,\tau_{10}) - M(\alpha_1,1,\tau_{10}))+\\&(U(\alpha_2,1,\tau_{21})M'(\alpha_1,1,\tau_{11}) - U'(\alpha_2,1,\tau_{21})M(\alpha_1,1,\tau_{11}))(2U'(\alpha_1,1,\tau_{10}) - U(\alpha_1,1,\tau_{10})) = 0\end{aligned} \tag{16}$$

Where U and M are the two linearly independent Confluent Hypergeometric functions and

$$\alpha_j = \frac{1}{2}\left(1 - \frac{\omega^2}{gk_{m,n}s_j}\right),\quad j = 1,2 \tag{17}$$

$$\tau_{j1} = \frac{2k_{m,n}}{s_j}\left(s_j x_1 + h_j\right),\quad j = 1,2 \tag{18}$$

$$\tau_{10} = \frac{2k_{m,n}}{s_1}h_1 \tag{19}$$

With ω the angular frequency and $k_{m,n} = \frac{m\pi}{2b},\ \ m = 1,2,3,\ldots$ indicating the eigenvalue of the m^{th} transverse oscillation mode. The constant slope bottom can be theoretically regarded as a special case of the two-slope-piecewise one when $s_1 = s_2$. It can be seen theoretically that the transverse oscillation components on a constant slope s and on a piecewise bottom with $s_1 = s$ share nearly the same theoretical frequencies for relatively low modes. With the values listed in the table, it is observed that the numerically calculated frequencies of the components are very close to the analytical ones, especially for the modes with both small m and small n. For the modes with larger n, as the corresponding wave profiles extend farther in the offshore direction, they may be subjected to a greater influence of the deepening of the water and the errors $|f_t - f_n|/f_t$ may reasonably become slightly larger. Well captured by the analytical solutions, the offshore profiles of the several principal components trapped within the harbor on each slope are represented in Fig. 6 and compared with those of the corresponding theoretical modes with the same amplitude at the backwall. It can be revealed from the comparisons of the seaward wave profiles that for the oscillations induced by vessel moving from the backwall all the way to the mouth of the harbor, higher modes in the offshore direction (with larger n) can be more easily exited than those in the longshore direction (with larger m) as the vessel itinerary traverse more antinodes of these higher offshore modes. For the mode with larger m (2,0), the appearance of traces of very small antinodes makes it deviate slightly from the theoretical curve at a certain distance away from the backwall and this may be imputed to the disturbances from the higher offshore modes oscillating at tightly surrounding frequencies.

4. Analysis of oscillations induced by vessel motions

From the frequency-domain analysis of numerical results presented in the validation cases for the harbor oscillations induced by vessel motions on two kinds of bottom, it is generally revealed that, similar to the oscillations generated by submerged sliding masses or other external disturbances, transverse oscillations occur as the principle components containing most of the oscillation energy inside the harbor with relatively weak longitudinal components situating in low-frequency region of the spectra. While the vessel moves right along one sidewall of the harbor from the backwall all the way to the entrance, the occurrence of the components as numerous as possible can be observed and as the transverse components are trapped modes, their oscillation energy may be maintained within the harbor whereas the longitudinal ones dissipate

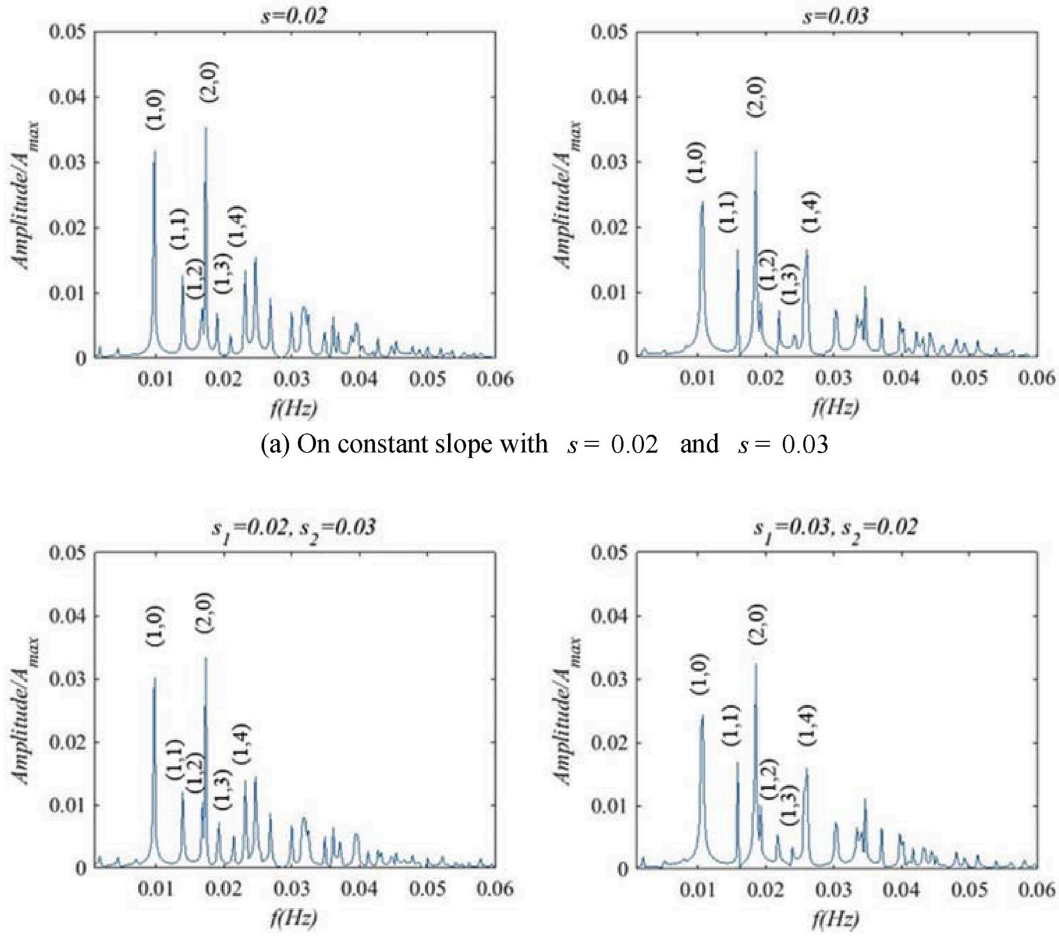

(a) On constant slope with $s = 0.02$ and $s = 0.03$

(b) On two-slope-piecewise bottom with $s_1 = 0.02, s_2 = 0.03$ and $s_1 = 0.03, s_2 = 0.02$

Fig. 5. Amplitude spectra at the corner of the semi-enclosed harbor (0 m,250 m) generated by the outgoing vessel along one sidewall, normalized by the maximum wave amplitude induced by the vessel motion.

Table 1
Comparison of oscillation frequencies of the principle modes occurring within the semi-enclosed harbor (with subscript *t* indicating the theoretical values and subscript *n* indicating the numerically simulated ones) and the relative deviations are shown in the last column in percentage.

Mode (m,n)	$k_{m,n}(m^{-1})$	$f_t(Hz)$	α_{1t}	$f_n(Hz)$	α_{1n}	$\lvert f_t - f_n\rvert/f_t(\%)$	
$s = 0.02$	(1,0)	0.00628	0.00981	−0.42473	0.00977	−0.41629	0.46
	(1,1)	0.00628	0.01414	−1.42012	0.01392	−1.36157	1.54
	(1,2)	0.00628	0.01659	−2.27225	0.01625	−2.22773	2.04
	(2,0)	0.01257	0.01700	−0.88865	0.01743	−0.94268	2.52
	(1,3)	0.01257	0.01929	−1.28749	0.01939	−1.24143	0.52
	(1,4)	0.01257	0.02133	−1.68472	0.02148	−1.61841	0.70
$s = 0.03$	(1,0)	0.00628	0.01069	−0.59795	0.01074	−0.60818	0.46
	(1,1)	0.00628	0.01606	−1.97772	0.01587	−1.91967	1.18
	(1,2)	0.00628	0.01956	−3.17435	0.01929	−3.07492	1.36
	(2,0)	0.01257	0.01861	−1.16432	0.01855	−1.15295	0.34
	(1,3)	0.01257	0.02223	−1.87311	0.02197	−1.81863	1.15
	(1,4)	0.01257	0.02603	−2.75578	0.02612	−2.77731	0.33
$s_1 = 0.02$	0.00628	0.00981	−0.42473	0.00977	−0.41629	0.46	
$s_2 = 0.03$(1,0)	(1,1)	0.00628	0.01414	−1.42012	0.01392	−1.36157	1.54
	(1,2)	0.00628	0.01699	−2.27225	0.01625	−2.22773	0.81
	(2,0)	0.01257	0.01749	−0.96982	0.01743	−0.95937	0.36
	(1,3)	0.01257	0.01929	−1.28749	0.01939	−1.30604	0.52
	(1,4)	0.01257	0.02133	−1.68472	0.02148	−1.71636	0.72
$s_1 = 0.03\, s_2 = 0.02$(1,0)	0.00628	0.01069	−0.59795	0.01074	−0.60818	0.46	
	(1,1)	0.00628	0.01606	−1.97772	0.01587	−1.91967	1.18
	(1,2)	0.00628	0.01956	−3.17577	0.01929	−3.07492	1.38
	(2,0)	0.01257	0.01861	−1.16432	0.01855	−1.15295	0.34
	(1,3)	0.01257	0.02224	−1.87529	0.02173	−1.76825	2.28
	(1,4)	0.01257	0.02440	−2.36042	0.02393	−2.25079	1.94

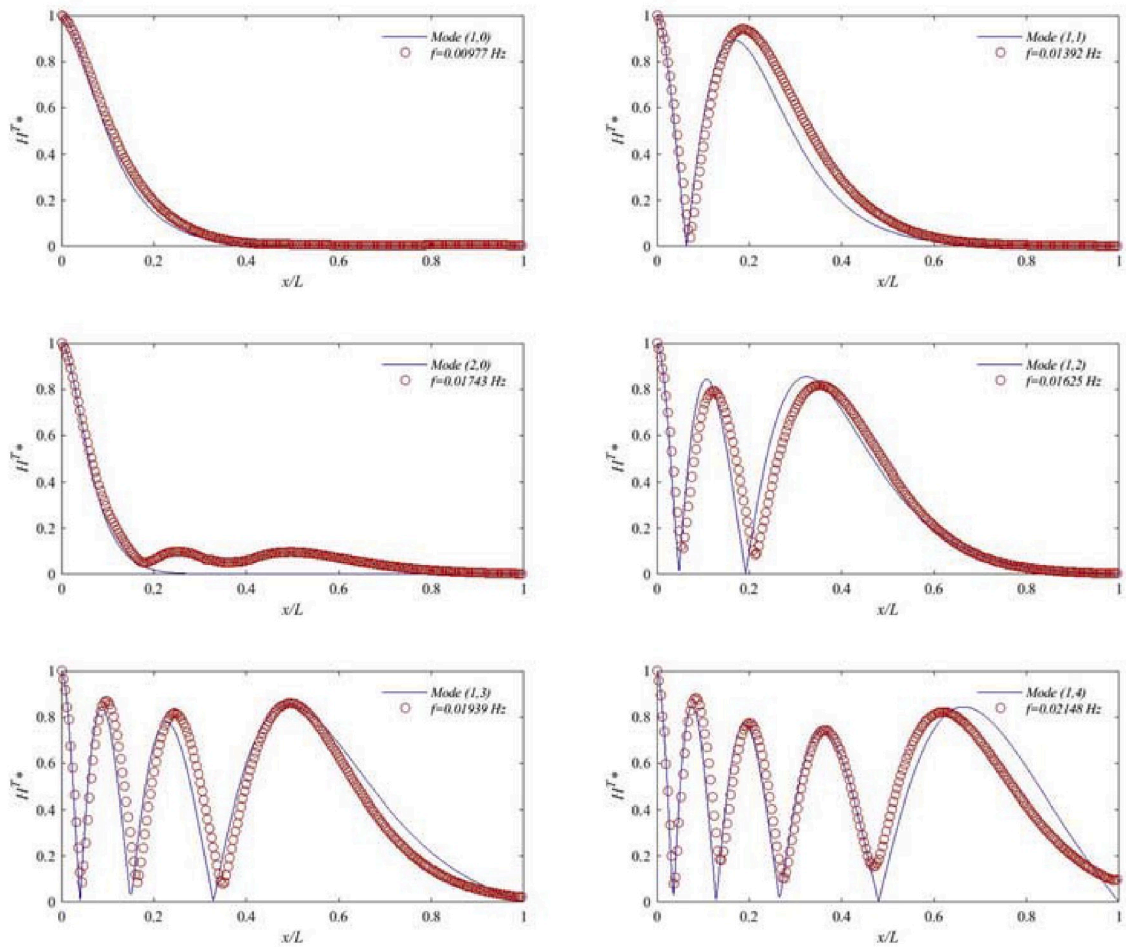

Fig. 6. Comparison of the numerically simulated offshore profiles of the several principal oscillation components (marked with red circles with their oscillation frequencies indicated in the legends) with theoretical ones (marked with blue solid lines with their mode numbers presented in the legends). (For interpretation of the references to color in this figure legend, the reader is referred to the Web version of this article.)

with the passage of time.

With the model settings indicated in the previous section, a range of numerical experiments are carried out to investigate the oscillations induced by various vessel motions with different harbor bathymetries by means of the conventional frequency-domain analysis method and in addition to which, the pattern recognition procedure proposed in Section 2 is employed onto the time series of the numerical simulations and thereby further examines the spatiotemporal characteristics of the oscillation behavior.

4.1. The effects of the changing vessel motions and harbor bathymetry (in frequency domain)

The analysis of the effects of the changing vessel motions and harbor bathymetry are in the first place carried out in frequency domain. With the same vessel motions as external excitation generating oscillations within the semi-enclosed harbor, the frequencies of the principle oscillation components with one or two nodes in the longshore direction which may contain most of the oscillation energy are reported in Fig. 7 for a variation of the bottom slope and water depth of the harbor. It is revealed that with an increasing water depth for the whole inner harbor area, either due to a steeper bottom slope (shown in Fig. 7(a)) or a deeper backwall water depth (shown in Fig. 7(b)), the frequencies of the oscillation components with different longshore and offshore mode number shift to larger values. Note that in case (b), as the changing backwall water depth may lead to an evenly changing water depth over the whole range of the harbor, the change of the frequencies of different offshore oscillation modes appears also nearly homogeneous when the backwall water depth increases from 5 m to 20 m, which conforms to the possible water depth for this kind of bathymetry in reality. On the other hand, while the bottom slope turns steeper shown in case (a), a more significant deepening may occur farther away from the backwall and in consequence the oscillation components with larger offshore mode number are subjected to influence of greater importance.

On the vessel side, it can be seen from Fig. 8 that the frequency domain behavior of the oscillations is in general insensitive to the variation of the moving speed of the vessel and also to the direction of the movement within the harbor. With merely infinitesimal change in the distribution of energy on the occurring oscillation modes shown by their relative amplitudes, almost all these oscillation modes keep their frequencies when the outgoing vessel along one sidewall of the harbor speeds up from 2 m/s to 10 m/s following the same path. Most of the oscillation modes remain stable when the moving vessel changes its direction from outward to inward, especially the ones with lower frequencies which embody a best part of the total oscillation energy within the harbor. When the oscillations are induced by vessel moving outside of the harbor at a certain distance from the entrance following a path parallel to the shoreline, their behaviors in frequency domain are quite different in comparison with those induced by the aforementioned outgoing vessel inside the harbor. Relatively important longitudinal modes occur over lower frequency range together with several transverse modes with larger offshore mode number, since the external

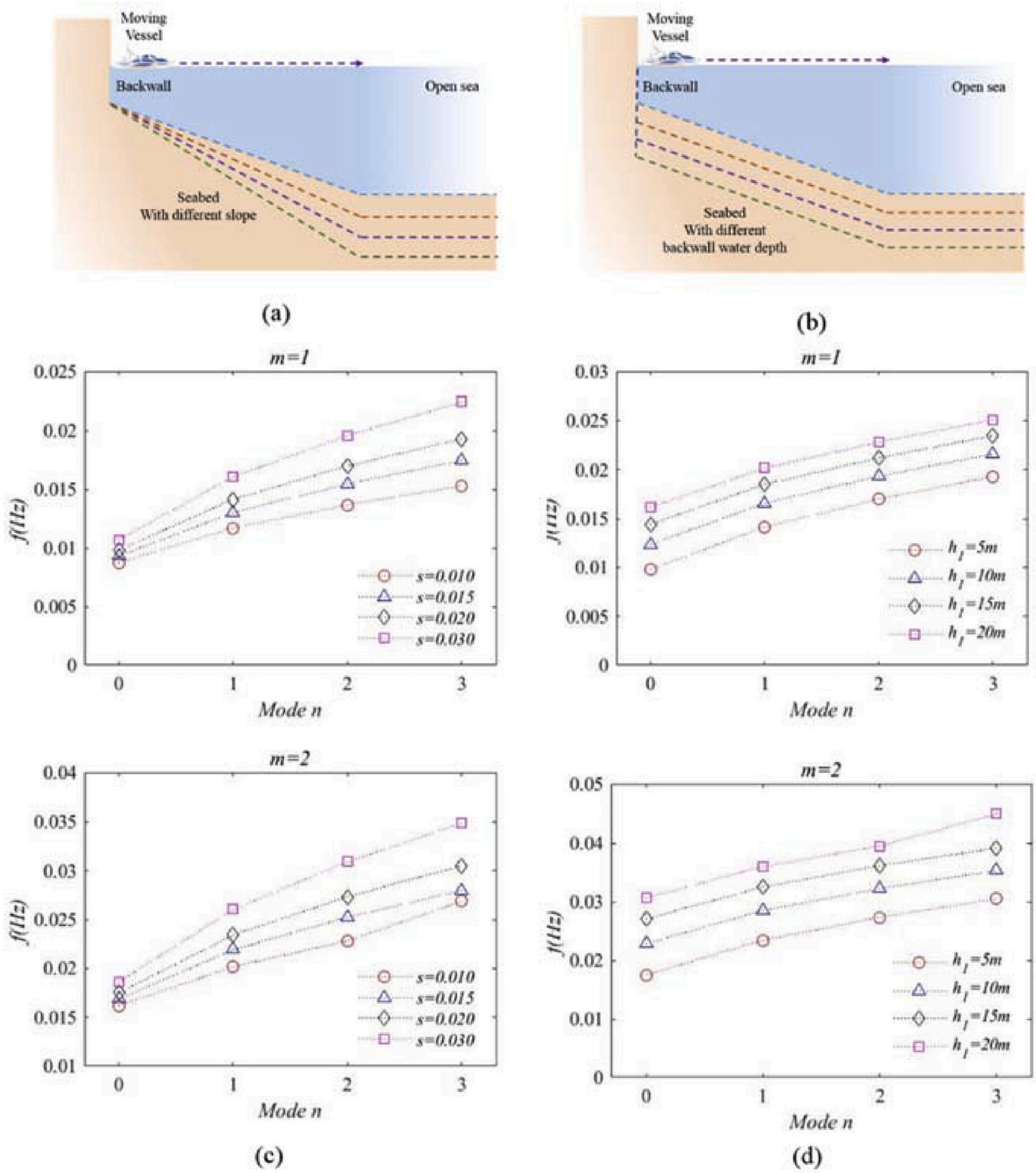

Fig. 7. Changing frequencies of the oscillation components with different longshore and offshore mode number with (a) the slope of bottom and (b) the water depth at backwall shown in (c) and (d) respectively.

disturbances come from outside of the harbor and the higher offshore modes may take precedence to be generated over lower ones whose oscillation energy is concentrated near the backwall of the harbor (farther away from the entrance).

4.2. Pattern recognition for the oscillation time series

It is revealed in the previous subsections that the changing vessel motions or harbor bathymetries can to some extent affect the frequency domain behavior of the induced oscillations. However, with their assumptions or approximations, the frequency domain analysis may sometimes fail to capture some characteristics of the oscillations which are in essence time series more or less unstable and it may also be interesting to know the time-domain behavior on its own and the proposed pattern recognition procedure is applied onto the recorded time series under different conditions. Following precedent threads of thought, the influencing factors on both the vessel side and the harbor side are examined and discussed. As what has been done in the previous subsection, on the harbor side, attention is focused on the slope and water depth of the harbor bathymetry. In the aspect of vessel motions, in addition to the effects of various moving speed, those of the itinerary of the vessel are also analyzed including comparisons between the vessel moving inwards or outwards the harbor and the itinerary being located within or outside of the harbor (shown in Fig. 8). The corresponding VAR coefficients of the oscillation time series with these changing conditions on the vessel side are plotted in Fig. 9.

Fig. 9(a) shows a distinct amount of variation in the VAR coefficients with a changing constant slope of the harbor bottom and the distinction seems mainly controlled by the first coefficient of the applied vector autoregressive moving average model. While the chosen values of the

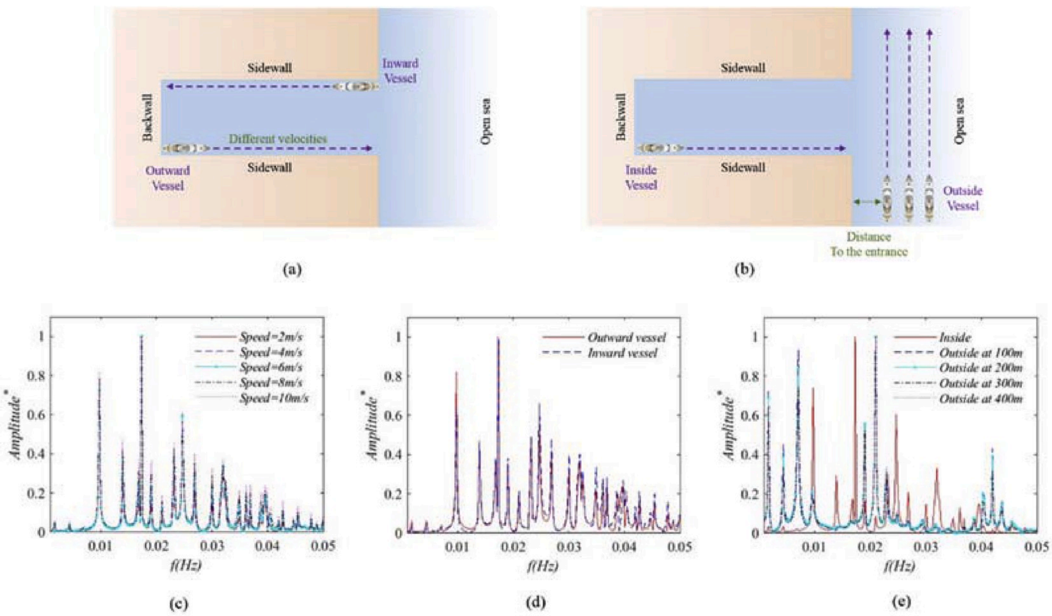

Fig. 8. Comparison between oscillations generated by different kind of vessel motions illustrated in (a) outward/inward vessel and (b) inside/outside vessel (at different distance to the harbor entrance) with the amplitude spectra at the corner of the semi-enclosed harbor (0 m,250 m) normalized by the maximum wave amplitude induced by the vessel motion shown in (c) for different vessel speed, (d) for outward/inward vessel and (e) for inside/outside vessel.

slope are mild and consistent with the realistic coastal bathymetries, it can be regarded that slight variations of the mild slopes may lead to a relatively apparent clustering of the VAR results of the recorded time series and thus the time-domain oscillation characteristics of the water surface within the semi-enclosed harbor. For a variation of water depth at the backwall of the harbor in Fig. 9(b) which can exist in reality for this kind of bathymetry, although the clustering seems less distinct than that for the bottom slope, a monotonic trend of the VAR results with regard to the first coefficient can be observed as shifting to smaller values when the water within the harbor becomes deeper. It is to a certain degree physically reasonable that the scatter points for different bottom slope disaggregate more intensively into groups than those for different backwall water depth since a varying bottom slope may change not only the inclination of the bottom surface itself but also the overall water depth within the harbor in the meantime, which can consequently change both resonance frequencies and amplitude profiles of the oscillation components induced by vessel motions. A similar monotonic trend can also be seen in the subplot (c) for the changing velocity of the vessel motions and the values of the first VAR coefficient are found to increase with a faster moving vessel. As the changing vessel speed mainly controls the agitation intensity of the ship wake which may merely influence the induced oscillation amplitudes therewith and the frequencies of almost of the oscillation modes remain the same (as reported in the previous subsection with frequency domain analysis), relatively limited clustering trends are observed. In addition, as the vessel may travel in both directions in entering and leaving the semi-enclosed harbor, simplified cases are considered (the vessel follows an inward and outward straight line as its moving path) and the consequent VAR results shown in Fig. 9(d) form two clusters which can be practically separated by a simple oblique line placed between them, which indicates that the time-domain oscillation patterns induced by the vessel motions in the two directions may differ from each other to a considerable extent. This observation is only captured with the pattern recognition presented here but fails to be found in the preceding frequency domain analysis. With a clear separation observed in Fig. 9(e) between the aggregation of the scatter points in red representing the VAR coefficients calculated for the oscillation time series induced by a seaward moving vessel departing from the backwall within the semi-enclosed harbor and that of the vessels traveling in the longshore direction outside of the harbor (marked in other colors), obvious difference between the time-domain patterns of the oscillations generated in the two different manners can be deduced, similar to what has been captured by the previous frequency domain analysis (Fig. 8(e)). As the moving vessel not only pushes the water in front of the stem but also forms a region of recirculating flow immediately behind the stern with the wave front of the wake patterns at a certain angle from the moving path, the direction and relative location of the vessel path or itinerary with regard to the spatial layout of the harbor may carry weight in the generation of the surrounding wave patterns within the harbor. However, for the three vessels traveling outside of the harbor entrance with their paths located parallel to each other at different exterior spacing, practically no distinct clustering can be found among the induced oscillations as different parallel paths of the vessel motions may have little impact on the propagation of the generated wave patterns, an observation also coinciding with the frequency domain results.

As the time series of the oscillation surface are measured at a variety of locations within the harbor, a clustering can also be seen in comparing the patterns from different locations and this kind of clustering can be more quantitatively illustrated by taking advantage of the distribution of probability density of the calculated Mahalanobis distances for the time series measured at different observation locations. Since it can be revealed from the analytical solutions (Shao et al., 2017a) that for the spatial profiles of different transverse oscillation modes, nodes and antinodes succeed each other in both the longshore and offshore directions, the time series recorded right at the nodes of a certain oscillation mode may not contain its information whereas those recorded at the antinodes can theoretically carry the information of this mode to its maximum. While all the oscillation modes may have their largest antinode right at the backwall of the semi-enclosed harbor in the offshore direction, the water surface time history at the backwall is chosen as a reference for the comparisons (for the modes with different n). Similarly, for the longshore direction, as the largest antinodes of all the modes with different m occur right at the sidewall where the water surface history can be chosen for comparisons in the longshore direction. Within the observed oscillations, close attention is given to the four lowest components with non-zero offshore nodes (with n from 1 to 4) as they may contain most of the perceptible resonance energy. For these oscillation components induced by a vessel moving outwards along one

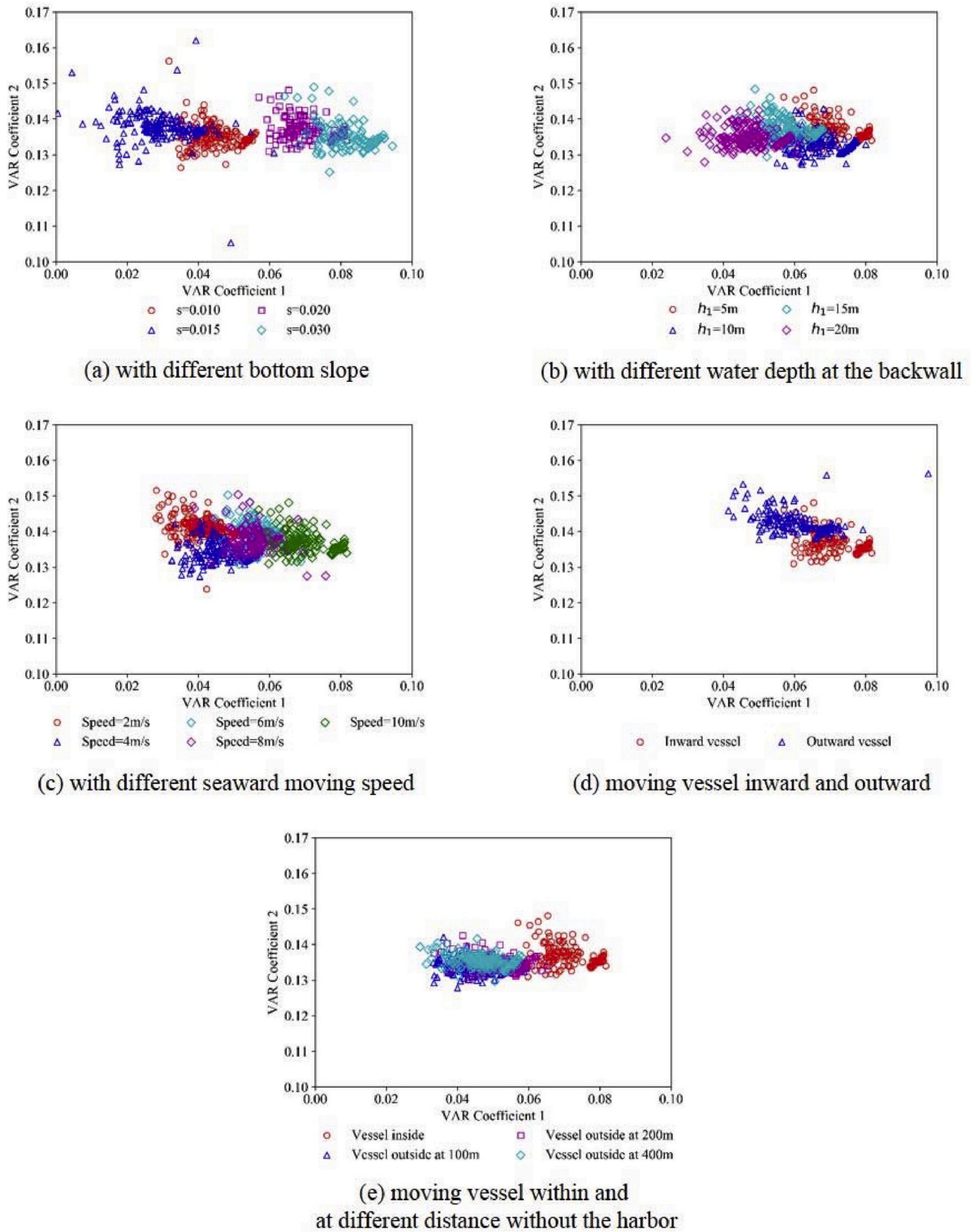

Fig. 9. Plotted VAR coefficients for the oscillation responses within the harbor induced by vessel motions for different conditions.

sidewall of the harbor on a constant slope $s = 0.02$, the positions of the nodes are listed in Table 2 which are extracted from the wave profiles in the results of the numerical simulations and these positions can also be well captured by theoretical solutions. Amplitude spectra in frequency domain obtained from the time series recorded at the nodes of these four components are shown in Fig. 10 in comparison with those obtained right at the backwall of the harbor and the deletions of the pic of corresponding mode are illustrated. Within the spectra, a reduction of the intensity of a certain lower oscillation modes can merely be seen with the attenuation of their pics when the oscillation time series are observed farther away from the backwall of the harbor on certain nodes of higher offshore modes (with larger mode number n) and from the superficial frequency-domain analysis and comparisons, little information can be further extracted.

The probability density of the calculated Mahalanobis distance for the first node (the only node) of mode $n = 1$ at 185 m, the second node of mode $n = 2$ at 530 m, the third node of mode $n = 3$ at 875 m and the fourth node of mode $n = 4$ at 1210 m are presented in Fig. 11(a). In general, the calculated probability densities can be fitted closely to normal distribution as can be seen from all the dotted fitting curves for

Table 2
Position of the offshore nodes for oscillation modes $n = 1, 2, 3, 4$ on constant slope with $s = 0.02$ and $s = 0.03$.

Mode n	Position from the backwall (m)							
	$s = 0.02$				$s = 0.03$			
1	185				160			
2	130	530			125	475		
3	115	410	875		100	370	820	
4	100	350	705	1210	90	325	670	1200

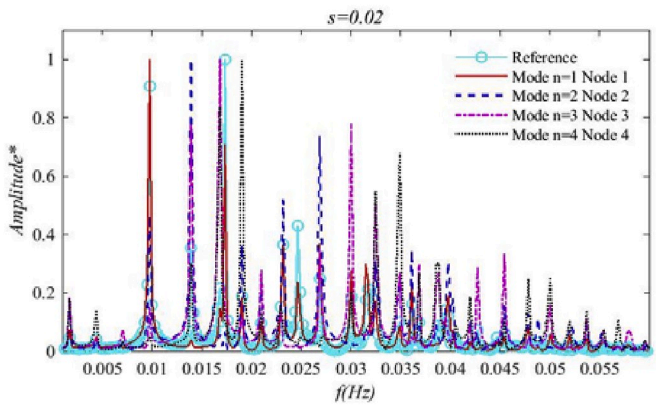

(a) For bottom slope $s = 0.02$

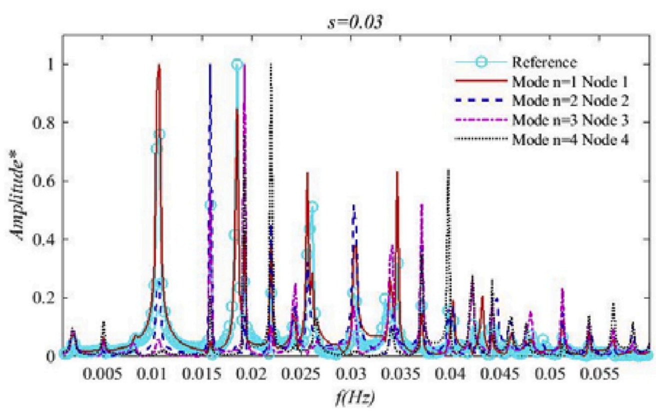

(b) For bottom slope $s = 0.03$

Fig. 10. Normalized amplitude spectra in frequency domain obtained from the time series recorded at the nodes of these four components in comparison with those recorded at the corner of the semi-enclosed harbor chosen as reference for two different slopes (with 'Amplitude*' indicating the normalized amplitudes with regard to the reference).

the four oscillation modes. The probability densities are concentrated towards larger Mahalanobis distance with nearly the same distribution width when the time series are recorded on nodes of higher offshore oscillation modes. As these chosen positions of the nodes recede from the backwall of the harbor one after another, it seems in a superficial manner that the concentration of the probability density tends to shift larger when they are recorded farther away in the offshore direction. However, when the Mahalanobis distances are calculated for mode $n = 2$ with the time history measured on the first node of this mode at only 130 m away from the backwall (closer than the second node at 530 m), the median of the fitted probability density bell-curve (blue dotted curve in Fig. 11(b)) moves on the contrary to larger Mahalanobis distance and tightly close to the medians of those for mode $n = 3$ and 4 respectively fitted by green and purple dotted curves. As it can be seen from Table 3 that the first node of mode $n = 2$ at 130 m is situated in the proximity of the first node of mode $n = 3$ and 4, it is reasonable that the Mahalanobis distances calculated from the time history here are significantly influenced by these two higher modes and may carry characteristics of these two modes. Similar phenomenon is revealed within the harbor of constant slope with $s = 0.03$ and the probability densities of the calculated Mahalanobis distance for the four principle offshore oscillation modes are shown in Fig. 12(a) and Fig. 12(b). The mean values and variances corresponding to the Mahalanobis distances of the time histories measured at the mentioned locations are listed in Table 3. In the meantime, another feature of the distribution of the probability density of the Mahalanobis distances may also be drawn from Figs. 11 and 12 for both bathymetries with different slope $s = 0.02$ and $s = 0.03$, which refers to a relative stagnation or stability of the bell-shape of the fitted curves when the observation points move onto the nodes of higher offshore oscillation modes (farther away seawards). In order to further elucidate this observation, the means and variances of the Mahalanobis distance calculated with regard to the reference for the time histories measured at the 250 observation points arranged in the manner as the OPs shown in Fig. 4 in the offshore direction from the backwall all the way to the harbor entrance are illustrated in Fig. 13. It is revealed that the mean values of the calculated Mahalanobis distances do not show a growing or downward trend but begin to level off at a certain distance away from the backwall. The means begin to converge towards a relatively fixe value of 1.5 in the second half of the harbor together with the variances approaching a value of 0.2. In addition, in the vicinity of the backwall, a monotonic tendency can neither be seen for the mean values nor for the variances from Fig. 13. The fluctuations in this part of the harbor together with the subsequent convergences near the mouth of harbor may to some extent show a conformity to the feature observed within the bell-shape curve in Figs. 11 and 12.

5. Conclusion

This study presents a novel sensitive harbor oscillation feature in the context of statistical pattern recognition to analyze the spatiotemporal oscillation behaviors induced by vessel motions within a harbor of variable water depth by taking advantage of the time-domain oscillation series, in addition to frequency domain analysis. In order to capture the vessel-induced oscillation behaviors from this perspective, vector autoregressive model is proposed to examine the recorded oscillation time histories of the water surface within the semi-enclosed harbor at different observation points and from which features are extracted by measuring the amount of deviations calculated with the selected VARMA coefficients.

As both the harbor bathymetry and the movements of the vessel may change the oscillation behavior, time series of the water surface induced on a variation of harbor bottom slope and inner-harbor water depth are investigated together with those generated with changing vessel motions with different velocity, traveling direction and location of the movements. Frequency-domain analysis show that the changing conditions in harbor bathymetry including the slope and water depth may have influence on the oscillation frequencies of different modes whereas a changing vessel direction or velocity may neither affect the mode frequencies nor the occurrence of different modes. However, the pattern recognition results on the basis of the time-domain series demonstrate that more or less distinct clustering of the VARMA coefficients can be observed not only for the time series with the changing conditions affecting a priori the frequency-domain behavior, but also for those with the changing conditions of little importance in frequency-domain analysis. Among all the conditions being investigated, a changing bottom slope may have the most significant influence on the time-domain behavior of the oscillations as it modifies both the water depth distribution and bottom profile within the harbor. For the vessel side, it is interestingly to note that palpable separation can be observed between the time-domain oscillation behaviors induced by a vessel traveling in

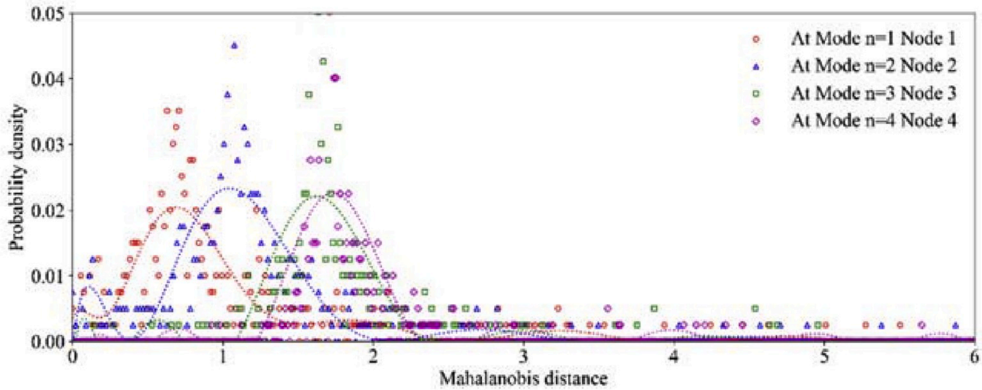

(a)

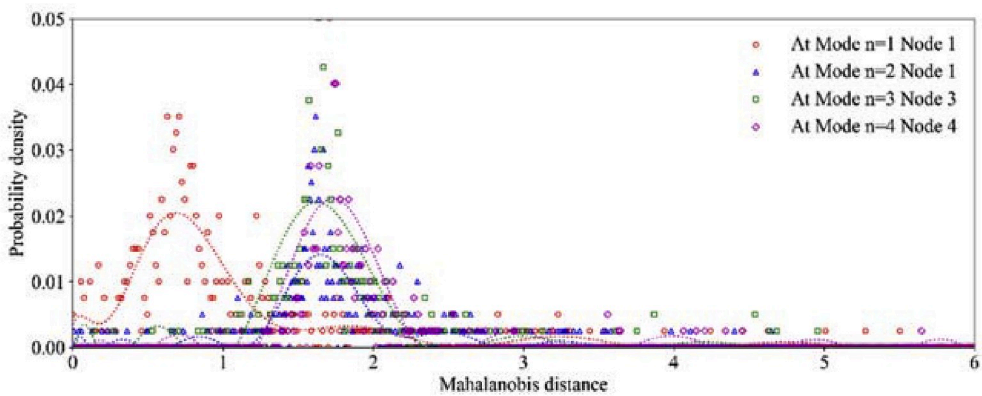

(b)

Fig. 11. Probability distribution of the calculated Mahalanobis distance for the four principle offshore oscillation modes within the harbor of constant slope s = 0.02 with (a) calculated with the time history measured on the 2nd node for Mode n = 2 and (b) calculated with the time history measured on the 1st node for Mode n = 2.

Table 3
Mean and variance for the Mahalanobis distances measured at locations corresponding to the offshore nodes of the principle transverse oscillation modes.

Location/Item	s = 0.02		s = 0.03	
	mean	variance	mean	variance
Mode n = 1 Node 1	1.108	1.113	1.156	1.161
Mode n = 2 Node 1	1.780	0.344	1.781	0.392
Mode n = 2 Node 2	1.279	1.089	1.526	0.775
Mode n = 3 Node 3	1.779	0.415	1.865	0.260
Mode n = 4 Node 4	1.860	0.275	1.906	0.183

different direction. The same kind of separation can also be found for those induced by a vessel moving inside or outside the harbor.

In addition to the responses of the harbor oscillations induced by vessel motions to variations of external conditions, the information of internal structure of the induced oscillations can also be revealed with the pattern recognition approach on account of the recorded time series at different observation locations. As a further step than the clustering analysis of the VARMA coefficients, Mahalanobis distances of them with regard to a reference and their probability density distribution are employed to investigate the spatial behavior of the oscillations in which the energy is contributed by different internal components (the resonance modes). While the profile of probability density distribution of the calculated Mahalanobis distances remains generally unchanged, the mean of these distances may to some extent illustrate the occurrence or absence of certain resonance components or modes in the internal structure of the oscillations within the harbor.

The proposed pattern recognition procedure in this study can be potentially applied to other nearshore hydrodynamic analysis especially for wave propagations or resonances and on more realistic coastal bathymetries. It should also be mentioned that the characteristics of the internal structure of the wave patterns may be revealed by a successful implementation of the proposed procedure in the requirement of time-domain measurements at multiple locations which are spatiotemporally correlated to each other in an intrinsic manner. In addition, although the investigations have been carried out in this study on the oscillations induced by vessel motions, different behaviors of oscillations or other wave patterns induced by other types of external forcing sources such as meteorological events and submerge landslides may also be potentially identified by implementing the proposed procedure.

Declaration of competing interest

The authors declare that they have no known competing financial interests or personal relationships that could have appeared to influence the work reported in this paper.

CRediT authorship contribution statement

Dong Shao: Conceptualization, Methodology, Formal analysis, Software, Investigation, Writing - original draft, Writing - review & editing. **Yun Xing:** Methodology, Validation, Supervision, Writing - original draft, Writing - review & editing, Visualization, Funding

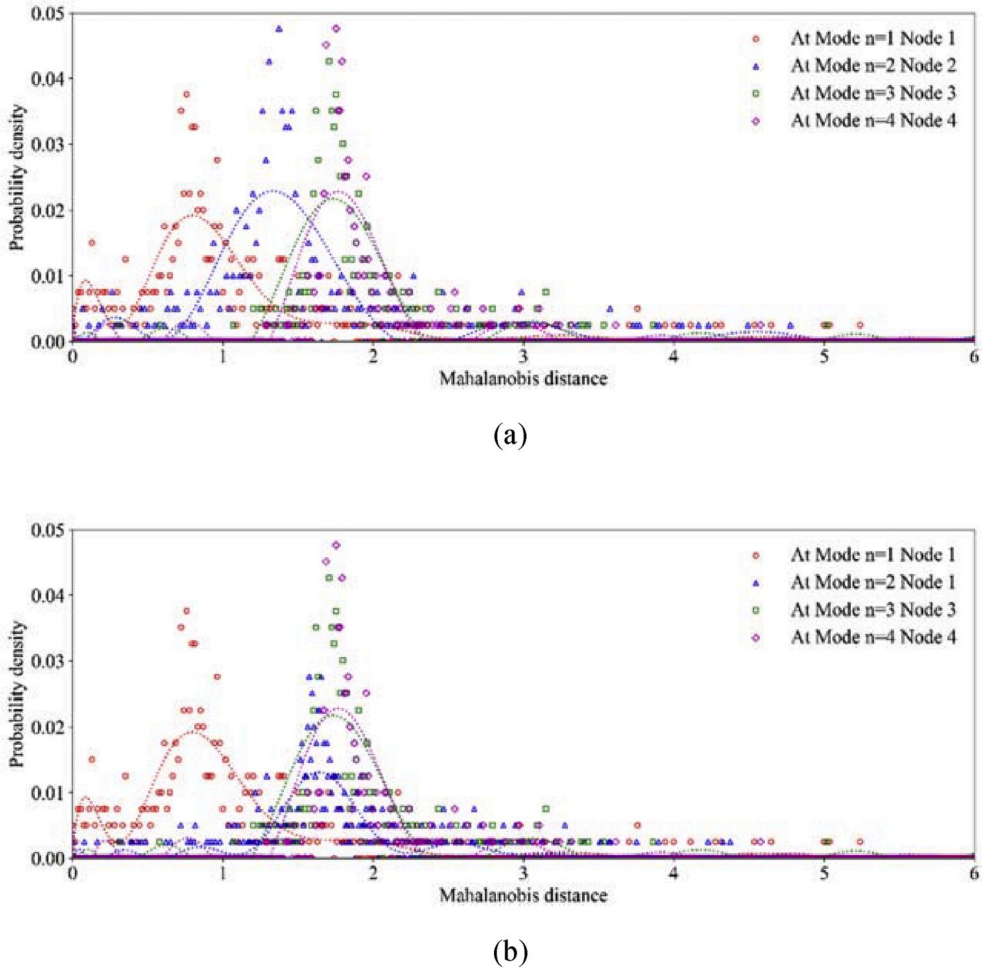

Fig. 12. Probability distribution of the calculated Mahalanobis distance for the four principle offshore oscillation modes within the harbor of constant slope s = 0.03 with (a) calculated with the time history measured on the 2nd node for Mode n = 2 and (b) calculated with the time history measured on the 1st node for Mode n = 2.

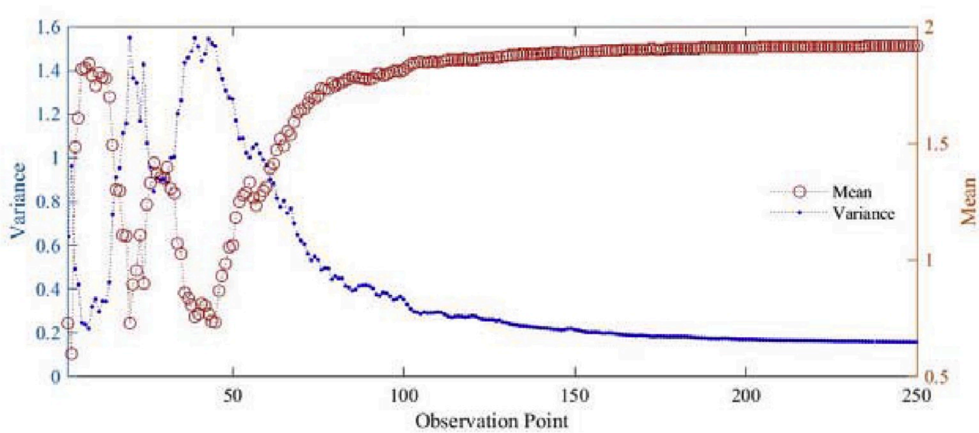

Fig. 13. The mean and variance of the Mahalanobis distances of the time histories measured at the 250 observation points in the offshore direction along one sidewall of the harbor with regard to that measured at the backwall corner chosen as reference.

acquisition. **Zirui Zheng:** Methodology, Software, Formal analysis, Investigation, Validation, Writing - review & editing. **Gang Jiang:** Supervision, Writing - review & editing, Funding acquisition.

Acknowledgements

This research was supported financially by the Natural Science Foundation of Jiangsu Province, China (BK20171468). The authors are also grateful for the discussions and suggestions given by the professors carrying out researches in the domain of structure health monitoring, from which the inspiration of this study is drawn.

References

Andersen, P., 1997. Identification of Civil Engineering Structures Using Vector ARMA Models. Department of Building technology and Structural Engineering.

Andersen, P., Brincker, R., 1998. Estimation of Modal Parameters and Their Uncertainties. Instituttet for Bygningsteknik, Aalborg Universitet.

Bellotti, G., 2007. Transient response of harbours to long waves under resonance conditions. Coast. Eng. 54 (9), 680–693.

Bodeux, J.-B., Golinval, J.-C., 2003. Modal identification and damage detection using the data-driven stochastic subspace and ARMAV methods. Mech. Syst. Signal Process. 17 (1), 83–89.

Box, G., Jenkins, G., Reinsel, G., 1994. Time Series Analysis- Forecasting and Control. Prentice-Hall, Englewood Cliffs, NJ, 1994.

Carden, E.P., Brownjohn, J.M., 2008. ARMA modelled time-series classification for structural health monitoring of civil infrastructure. Mech. Syst. Signal Process. 22 (2), 295–314.

Chen, G.-Y., Chien, C.-C., Su, C.-H., Tseng, H.-M., 2004. Resonance induced by edge waves in Hua-Lien Harbor. J. Oceanogr. 60 (6), 1035–1043.

Chen, M.-Y., Mei, C.C., Chang, C.-K., 2006. Low-frequency spectra in a harbour excited by short and random incident waves. J. Fluid Mech. 563, 261–281.

Chen, Q., 2006. Fully nonlinear Boussinesq-type equations for waves and currents over porous beds. J. Eng. Mech. 132 (2), 220–230.

Das, S., Saha, P., Patro, S., 2016. Vibration-based damage detection techniques used for health monitoring of structures: a review. J. Civ. Struct. Health Monit. 6 (3), 477–507.

De Girolamo, P., 1996. An experiment on harbour resonance induced by incident regular waves and irregular short waves. Coast. Eng. 27 (1–2), 47–66.

Degtyarev, A., Gankevich, I., 2015. Hydrodynamic pressure computation under real sea surface on basis of autoregressive model of irregular waves. Phys. Part. Nucl. Lett. 12 (3), 389–391.

Degtyarev, A.B., Gankevich, I., 2019. Contemporary Ideas on Ship Stability. Springer, pp. 37–47.

Degtyarev, A.B., Reed, A.M., Mareev, V., 2019. Contemporary Ideas on Ship Stability. Springer, pp. 25–35.

Dong, G., Wang, G., Ma, X., Ma, Y., 2010a. Harbor resonance induced by subaerial landslide-generated impact waves. Ocean Eng. 37 (10), 927–934.

Dong, G., Wang, G., Ma, X., Ma, Y., 2010b. Numerical study of transient nonlinear harbor resonance. Sci. China Technol. Sci. 53 (2), 558–565.

Erduran, K., Ilic, S., Kutija, V., 2005. Hybrid finite-volume finite-difference scheme for the solution of Boussinesq equations. Int. J. Numer. Methods Fluid. 49 (11), 1213–1232.

Ertekin, R., Webster, W., Wehausen, J., 1986. Waves caused by a moving disturbance in a shallow channel of finite width. J. Fluid Mech. 169, 275–292.

Fusco, F., Ringwood, J.V., 2010. Short-term wave forecasting for real-time control of wave energy converters. IEEE Trans. Sustain. Energy 1 (2), 99–106.

Gankevich, I., Degtyarev, A., 2018. The Ocean in Motion. Springer, pp. 249–278.

Gao, J., Ji, C., Gaidai, O., Liu, Y., 2016. Numerical study of infragravity waves amplification during harbor resonance. Ocean Eng. 116, 90–100.

Gao, J., Ji, C., Gaidai, O., Liu, Y., Ma, X., 2017. Numerical investigation of transient harbor oscillations induced by N-waves. Coast. Eng. 125, 119–131.

Gao, J., Ji, C., Liu, Y., Ma, X., Gaidai, O., 2018a. Numerical study on transient harbor oscillations induced by successive solitary waves. Ocean Dynam. 68 (2), 193–209.

Gao, J., Ma, X., Dong, G., Zang, J., Ma, Y., Zhou, L., 2019a. Effects of offshore fringing reefs on the transient harbor resonance excited by solitary waves. Ocean Eng. 190, 106422.

Gao, J., Ma, X., Dong, G., Zang, J., Zhou, X., Zhou, L., 2019b. Topographic influences on transient harbor oscillations excited by N-waves. Ocean Eng. 192, 106548.

Gao, J., Zhou, X., Zhou, L., Zang, J., Chen, Q., Ding, H., 2018b. Numerical study of harbor oscillations induced by water surface disturbances within harbors of constant depth. Ocean Dynam. 68 (12), 1663–1681.

González-Marco, D., Sierra, J.P., de Ybarra, O.F., Sánchez-Arcilla, A., 2008. Implications of long waves in harbor management: the Gijón port case study. Ocean Coast Manag. 51 (2), 180–201.

Gottlieb, S., Shu, C.-W., Tadmor, E., 2001. Strong stability-preserving high-order time discretization methods. SIAM Rev. 43 (1), 89–112.

Gul, M., Catbas, F.N., 2009. Statistical pattern recognition for Structural Health Monitoring using time series modeling: theory and experimental verifications. Mech. Syst. Signal Process. 23 (7), 2192–2204.

Gul, M., Catbas, F.N., 2011. Structural health monitoring and damage assessment using a novel time series analysis methodology with sensor clustering. J. Sound Vib. 330 (6), 1196–1210.

Havelock, T.H., 1908. The propagation of groups of waves in dispersive media, with application to waves on water produced by a travelling disturbance. Proc. R. Soc. Lond. - Ser. A Contain. Pap. a Math. Phys. Character 81 (549), 398–430.

Heyns, P., 1997. Structural damage assessment using response-only measurements. In: Structural Damage Assessment Using Advanced Signal Processing Procedures, Proceedings of DAMAS, vol. 97. Univ. of Sheffield, UK, pp. 213–223.

Hoell, S., Omenzetter, P., 2016. Optimal selection of autoregressive model coefficients for early damage detectability with an application to wind turbine blades. Mech. Syst. Signal Process. 70, 557–577.

Jäger, W.S., Nagler, T., Czado, C., McCall, R.T., 2019. A statistical simulation method for joint time series of non-stationary hourly wave parameters. Coast. Eng. 146, 14–31.

Jayawardhana, M., Zhu, X., Liyanapathirana, R., Gunawardana, U., 2015. Statistical damage sensitive feature for structural damage detection using AR model coefficients. Adv. Struct. Eng. 18 (10), 1551–1562.

Kakinuma, T., Toyofuku, T., Inoue, T., 2009. In: Proceedings of Coastal Dynamics 2009: Impacts of Human Activities on Dynamic Coastal Processes (With CD-ROM). World Scientific, pp. 1–11.

Kankal, M., Yüksek, Ö., 2012. Artificial neural network approach for assessing harbor tranquility: the case of Trabzon Yacht Harbor, Turkey. Appl. Ocean Res. 38, 23–31.

Kankal, M., Yüksek, Ö., 2014. Artificial neural network for estimation of harbor oscillation in a cargo harbor basin. Neural Comput. Appl. 25 (1), 95–103.

Kennedy, A.B., Kirby, J.T., Chen, Q., Dalrymple, R.A., 2001. Boussinesq-type equations with improved nonlinear performance. Wave Motion 33 (3), 225–243.

Kirby, J.T., 2016. Boussinesq Models and Their Application to Coastal Processes across a Wide Range of Scales. American Society of Civil Engineers.

Kirby, J.T., Shi, F., Tehranirad, B., Harris, J.C., Grilli, S.T., 2013. Dispersive tsunami waves in the ocean: model equations and sensitivity to dispersion and Coriolis effects. Ocean Model. 62, 39–55.

Kirby, J.T., Wei, G., Chen, Q., Kennedy, A.B., Dalrymple, R.A., 1998. FUNWAVE 1.0: Fully Nonlinear Boussinesq Wave Model-Documentation and User's Manual. Research Report NO. CACR-98-06.

Kofoed-Hansen, H., Kerper, D.R., Sørensen, O.R., Kirkegaard, J., 2005. Simulation of Long Wave Agitation in Ports and Harbours Using a Time-Domain Boussinesq Model.

Kulikov, E.A., Rabinovich, A.B., Thomson, R.E., Bornhold, B.D., 1996. The landslide tsunami of November 3, 1994, Skagway harbor, Alaska. J. Geophys. Res.: Oceans 101 (C3), 6609–6615.

Kumar, P., 2017. Extreme wave-induced oscillation in Paradip Port under the resonance conditions. Pure Appl. Geophys. 174 (12), 4501–4516.

Kumar, P., Zhang, H., Kim, K.I., 2014. Spectral density analysis for wave characteristics in Pohang New Harbor. Pure Appl. Geophys. 171 (7), 1169–1185.

Kumar, P., Zhang, H., Kim, K.I., Yuen, D.A., 2016. Modeling wave and spectral characteristics of moored ship motion in Pohang New Harbor under the resonance conditions. Ocean Eng. 119, 101–113.

Ljung, L., 1987. In: Kailath, T. (Ed.), System Identification {Theory for the User. Prentice Hall Information and System Sciences Serie. Englewood Cli s, NJ.

Londhe, S., Deo, M., 2004. Artificial neural networks for wave propagation. J. Coast Res. 1061–1069.

Losada, I.J., Gonzalez-Ondina, J.M., Diaz-Hernandez, G., Gonzalez, E.M., 2008. Numerical modeling of nonlinear resonance of semi-enclosed water bodies: description and experimental validation. Coast. Eng. 55 (1), 21–34.

Lynett, P.J., Gately, K., Wilson, R., Montoya, L., Arcas, D., Aytore, B., Bai, Y., Bricker, J. D., Castro, M.J., Cheung, K.F., 2017. Inter-model analysis of tsunami-induced coastal currents. Ocean Model. 114, 14–32.

Mei, C.C., Agnon, Y., 1989. Long-period oscillations in a harbour induced by incident short waves. J. Fluid Mech. 208, 595–608.

Owen, J., Eccles, B., Choo, B., Woodings, M., 2001. The application of auto–regressive time series modelling for the time–frequency analysis of civil engineering structures. Eng. Struct. 23 (5), 521–536.

Pandit, S.M., Wu, S.-M., 1983. Time Series and System Analysis with Applications. Wiley, New York.

Rabinovich, A.B., 2010. Handbook of Coastal and Ocean Engineering. World Scientific, pp. 193–236.

Reed, A.M., Degtyarev, A.B., Gankevich, I., Weems, K., 2016. New Models of Irregular Waves—Way Forward, pp. 95–102.

Schwarz, G., 1978. Estimating the dimension of a model. Ann. Stat. 6 (2), 461–464.

Shao, D., Feng, X., Feng, W., 2016. Numerical investigation of oscillations within a harbor of parabolic bottom induced by water surface disturbances. Appl. Ocean Res. 59, 153–164.

Shao, D., Feng, X., Feng, W., Hong, G., 2017a. Harbor oscillations on a piecewise bottom of two different slopes. J. Mar. Sci. Technol. 22 (4), 633–654.

Shao, D., Feng, X., Feng, W., Hong, G., 2017b. Numerical investigation of oscillations induced by submerged sliding masses within a harbor of constant slope. Appl. Ocean Res. 63, 49–64.

Shi, F., Kirby, J.T., Harris, J.C., Geiman, J.D., Grilli, S.T., 2012a. A high-order adaptive time-stepping TVD solver for Boussinesq modeling of breaking waves and coastal inundation. Ocean Model. 43, 36–51.

Shi, F., Ma, G., Kirby, J.T., Hsu, T.-J.T., 2012b. Application of a TVD solver in a suite of coastal engineering models. Coast. Eng. Proc. 1 (33), 31.

Sohn, H., Czarnecki, J.A., Farrar, C.R., 2000. Structural health monitoring using statistical process control. J. Struct. Eng. 126 (11), 1356–1363.

Tehranirad, B., Shi, F., Kirby, J.T., Harris, J.C., Grilli, S., 2011. Tsunami Benchmark Results for Fully Nonlinear Boussinesq Wave Model FUNWAVE-TVD, Version 1.0. Center for Applied Coastal Research, University of Delaware, pp. 14–38.

Thotagamuwage, D.T., Pattiaratchi, C.B., 2014a. Influence of offshore topography on infragravity period oscillations in Two Rocks Marina, Western Australia. Coast. Eng. 91, 220–230.

Thotagamuwage, D.T., Pattiaratchi, C.B., 2014b. Observations of infragravity period oscillations in a small marina. Ocean Eng. 88, 435–445.

Torsvik, T., Pedersen, G., Dysthe, K., 2008. Influence of cross channel depth variation on ship wave patterns. Preprint Series. Mechanics and Applied Mathematics. http://urn.nb.no/URN:NBN:no-23418.

Vanem, E., Walker, S.-E., 2013. Identifying trends in the ocean wave climate by time series analyses of significant wave heightdata. Ocean Eng. 61, 148–160.

Vanoni, V.A., Carr, J.H., 1950. Harbor surging. Coast. Eng. Proc. 1 (1), 6.

Wang, G., Dong, G., Perlin, M., Ma, X., Ma, Y., 2011. Numerical investigation of oscillations within a harbor of constant slope induced by seafloor movements. Ocean Eng. 38 (17–18), 2151–2161.

Wu, T.Y.-T., 1987. Generation of upstream advancing solitons by moving disturbances. J. Fluid Mech. 184, 75–99.

Yalciner, A.C., Pelinovsky, E.N., 2007. A short cut numerical method for determination of periods of free oscillations for basins with irregular geometry and bathymetry. Ocean Eng. 34 (5–6), 747–757.

Yao, R., Pakzad, S.N., 2012. Autoregressive statistical pattern recognition algorithms for damage detection in civil structures. Mech. Syst. Signal Process. 31, 355–368.

Zhang, X., Li, D., Song, G., 2018. Structure damage identification based on regularized ARMA time series model under environmental excitation. Vibration 1 (1), 138–156.